Correlation between Resistance and Field Emission Performance of Individual ZnO One-Dimensional Nanostructures

Juncong She, Zhiming Xiao, Yuhua Yang, Shaozhi Deng, Jun Chen, Guowei Yang,* and Ningsheng Xu*

State Key Laboratory of Optoelectronic Materials and Technologies, and Guangdong Province Key Laboratory of Display Material and Technology, School of Physics and Engineering, Sun Yat-sen University, Guangzhou 510275, People's Republic of China

ABSTRACT Both electrical and field emission measurements were carried out to study the correlation between resistance and field emission performance of individual one-dimensional (1D) ZnO nanostructures. Three types of 1D ZnO nanostructures were investigated (*i.e.*, agave-like shape, pencil-like shape, and hierarchical structure) and were prepared by thermal chemical vapor transport and condensation without using any catalyst. The 1D ZnO nanostructures have obvious differences in resistance and thus conductivity from type to type. In addition, in the same type of 1D ZnO nanostructure, each individual emitter may also have variation in resistance and thus in conductivity. The field emission performance of the ZnO emitters was found to be strongly correlated with the resistance of each individual ZnO nanostructure: (i) a ZnO emitter with low resistance will have better emission; (ii) a high resistance region in a ZnO nanostructure is liable to the initiation of a vacuum breakdown event. The results indicate that, besides the uniformity in the geometrical structure, the uniformity in conductivity of the emitters in an array should be ensured, in order to meet the requirement of device application.

KEYWORDS: single ZnO nanostructure · field emission · anode probe · resistance · vacuum breakdown

Recently, a number of studies have been performed on the growth and the field emission properties of one-dimensional (1D) ZnO nanostructures,[1−13] with one interest in exploiting their possible application in vacuum micro/nanoelectronics[1−5] and another in understanding the underlying physical processes involved.[6−11] Already, efforts have been devoted to investigating effects on field emission of the density,[6] the geometrical structure,[7−9] the surface electrical potential barrier,[10] and the n-type doping[11] of ZnO nanowires/nanorods. Most of the measurements performed so far used ZnO nanostructure films, and thus the results represent the collective behaviors of the field emitter arrays. Only a few studies[14−16] were done on individual single ZnO field emitters. For example, Ramgir *et al.*[14] measured the current−voltage (*I*−*V*) behavior and work function of the multipod ZnO nanostructures. Yeong *et al.*[15] studied the effects of O_2 and H_2 exposures and ultraviolet illumination on the field emission properties of individual ZnO nanoemitters. Huang *et al.*[16] reported the dependence of the field enhancement factor on the distance between the nanostructure tip and its counteranode. However, there is an important physical factor that has not been investigated, that is, the effect of the resistance/conductivity of an individual ZnO emitter on its field emission performance. The resistance of the emitter governs the supply of the emitted electron. In addition, due to joule heating, an emitter with large resistance may be more liable to initiating a vacuum breakdown. Therefore, it is an issue of significant scientific and technological importance for exploring the correlation between the resistance and the field emission performance of the individual 1D ZnO nanostructures. The knowledge will be useful for the development of a ZnO nanostructure-based cathode for high performance vacuum micro/nanoelectronic devices.

RESULTS AND DISCUSSION

The 1D ZnO nanostructures studied are agave-like structures, pencil-like structures, and hierarchical structures.[7,17−19] Figure 1 gives the typical scanning electron microscopy (SEM, Raith e-line) images of the 1D nanostructures and their corresponding geometrical models. In SEM investigations, it was found that (i) the agave-like structure is in tip shape; (ii) the hierarchical structure consist of two parts: a nanowire on the top of a microcolumn; (iii) the pencil-like structure has the trunk with a tip on top. The images obtained using high-resolution transmission electron microscope (HRTEM, FEI Technai F30) (Figure 2) show that the nanostructures are well crystallized and the growth directions are the same, that is, along the [0001] direction. It is believed

*Address correspondence to stsxns@mail.sysu.edu.cn, stsygw@mail.sysu.edu.cn.

Received for review May 12, 2008 and accepted September 03, 2008.

Published online September 12, 2008.
10.1021/nn800283u CCC: $40.75

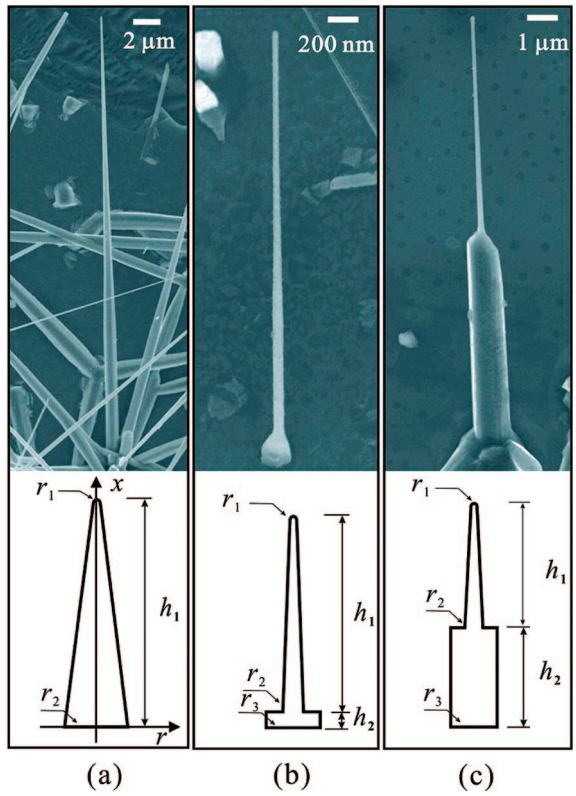

Figure 1. Typical SEM images and the corresponding geometrical models of the 1D nanostructures: (a) agave-like structure, r_1 and r_2 are the radius of the tip and the bottom, respectively, h_1 is the length; (b) hierarchical structure, r_1 is the radius of the nanowire and r_2 is the radius of the microcolumn, h_1 and h_2 are the length of each part; (c) pencil-like structure, r_1 and r_2 are the radius of the tip and the bottom of the trunk, r_3 is the radius of the microcolumn, h_1 and h_2 are the length of each part.

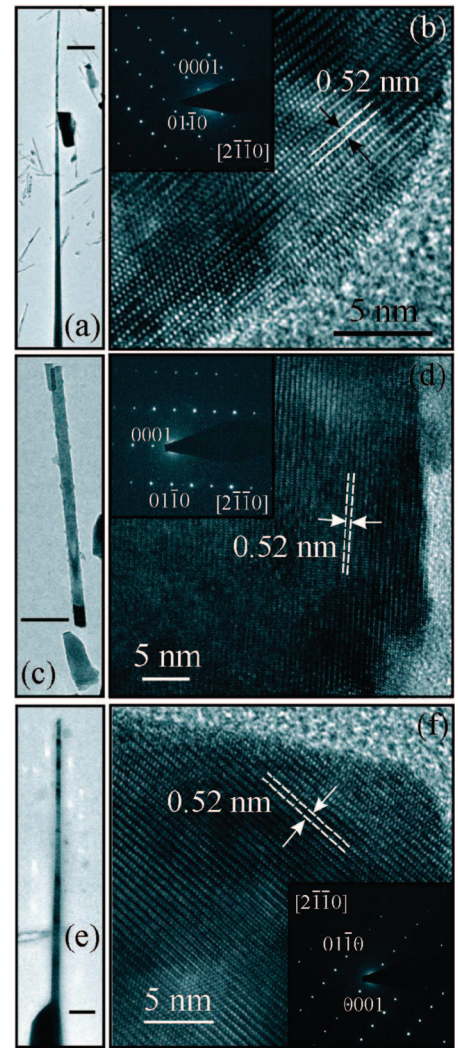

Figure 2. Typical HRTEM images of the apex regions of the 1D nanostructures: (a and b) the agave-like structure; (c and d) the hierarchical structure, (e and f) the pencil-like structure.

that the 1D nanostructures were formed due to the immiscible effect between the ZnO and a-C film. The ZnO concentration of the growth ambience was expected to play a crucial role in the shape controlling.[19] Presently, it is still not yet possible to control the diameter based on our current catalyst-free method.

Five individual 1D ZnO nanostructures for each type were studied. Their geometrical parameters are listed in Table I. Figure 3 shows the typical $I-V$ curves from the contact electrical measurements of three types of 1D nanostructure. They show distinct $I-V$ characteristics. (i) Linear $I-V$ and large values of current between 3.27 and 552 nA were obtained from four of the agave-like structures (Figure 3a). (ii) Four hierarchical structures exhibit nonlinear $I-V$ characteristics with small values of current between 60 pA and 2.7 nA (Figure 3b). (iii) Very small values of current of <20 pA were recorded from the pencil-like structures (Figure 3c), except one with a current of 3.9 nA. The resistance of the 1D ZnO nanostructures can be estimated from the $I-V$ curves,[20,21] which are given in Table I. Generally, the three types of 1D ZnO nanostructures have obvious differences in resistance. In addition, in the same type of 1D ZnO nanostructure, though the resistances values are varied, they have fallen in a relative narrow range as compared to that between different types of nanostructures.

Field emission measurements were carried out after the resistance measurements. The anode−cathode separation was adjusted to be ~2 μm. It was found that the field emission properties of various types of ZnO 1D nanostructures are distinctly different. For all the pencil-like nanostructures tested, no discernible field emission current was observed even when the applied voltage was increased to a very high value of 500 V (corresponding to an electric field of 250 MV/m). SEM observation found that the nanostructures were broken after the field emission measurement (Figure 4b). For both the agave-like and the hierarchical nanostructures, field emission currents were recorded from those with relative lower resistance (*i.e.*, No. 1 to 4 nanostructures for the agave-like and the hierarchical). The typical field emission current−voltage ($I-V$) curves are given in Figure 5a,b. The corresponding

TABLE I. Parameters Used for the Simulations and the Values of Electric Field Intensities Obtained (the parameters of h_1, h_2, r_1, r_2, and r_3 are corresponding to the model given in Figure 1)

nanostructures		r_1 (nm)	r_2 (nm)	r_3 (nm)	h_1 (μm)	h_2 (μm)	E_{apex} (MV/m)	R (MΩ)	V_{th} (V)
agave-like	No.1	90	250	—	29.6	—	560.5	0.92	191
	No.2	66	345	—	35.7	—	627.4	2.33	183
	No.3	100	290	—	64	—	532.7	3.38	215
	No.4	67	675	—	33.5	—	714.8	292.87	217
	No.5	61	205	—	43.3	—	816.1	3.68×10^5	—
hierarchical	No.1	33	40	106	1.86	0.228	1255	277	215
	No.2	29.5	41	91.8	2.38	0.258	891	442	255
	No.3	22	45	88.7	2.6	0.227	1220	2.76×10^3	350
	No.4	48	61	96.5	2.47	0.214	900	1.54×10^4	397
	No.5	59.5	65	121	1.96	0.241	465.6	4.10×10^5	—
pencil-like	No.1	56	103	344	4.72	4	768.2	2.50×10^2	—
	No.2	62	156	312	6.97	3.6	699.3	2.63×10^6	—
	No.3	65.5	258.5	490	6.71	3.9	717.6	5.53×10^4	—
	No.4	72	133	444.5	3.69	6.49	641.5	1.05×10^5	—
	No.5	68	218.5	407.5	3.83	4.67	594.4	1.00×10^7	—

Folwer−Norheim (F−N) plots are indicated as insets. A threshold voltage (V_{th}, a voltage needed for obtaining an emission current of 50 nA) is defined for evaluating the field emission performance of the emitters. The V_{th} values are also listed in Table I. In addition, it was found that no field emission was detected from the nanostructures with very high resistance (*i.e.*, No. 5 nanostructure for the agave-like and the hierarchical). For these two nanostructures, vacuum breakdown phenomenon (Figure 4d,f) was observed. These breakdown events were catastrophic. Moreover, for exploring the limitation in the maximum emission current of the individual ZnO emitters (No. 1 to 4 nanostructures for the agave-like and the hierarchical), the applied voltages were gradually increased until the emitters failed. This failure was identified by a sudden vanish in emission current. *In situ* SEM observation revealed that the agave-like emitters were shortened (Figure 6b). However, the hierarchical emitters were completely destroyed (Figure 6d).

The inhomogeneity in field emission properties of the 1D emitters may result from several possible origins, for example, the surface work function, the electrical field intensity at emitter apex (E_{apex}), and the resistance of the emitter. By considering the fact that the ZnO 1D nanostructures are well crystallized (Figure 2), their surface work functions may be similar.[22] Therefore, we propose the following discussions for understanding the physical origins of our experimental observations, mainly on the effects of E_{apex} and the resistance.

For the nanostructures we studied, their geometrical parameters (*i.e.*, the height, the diameter, and the apex curvature radius) are varied. It is well-known that the aspect ratio of the emitters may affect the field intensity on the emitting surface. Thus, numerical simulations were carried out to calculate the E_{apex} for each type of 1D ZnO nanostructures. A computer code of "Quickfield" (version 5.0)[23] was employed. The model set up for the simulation is a point (anode probe)-to-

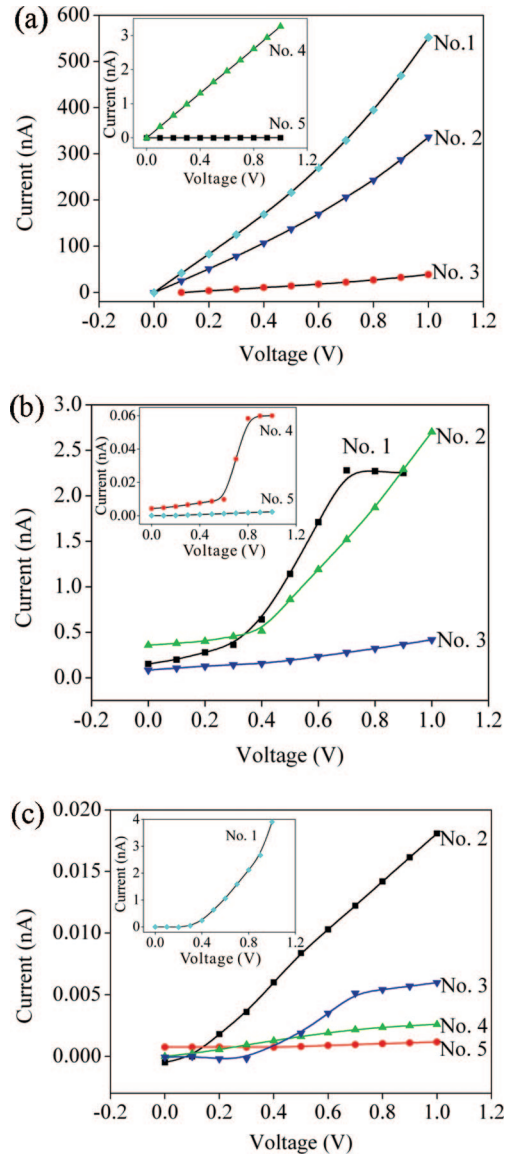

Figure 3. Typical *I*−*V* curves of the agave-like (a), the hierarchical (b), and the pencil-like structures (c) in electrical measurement.

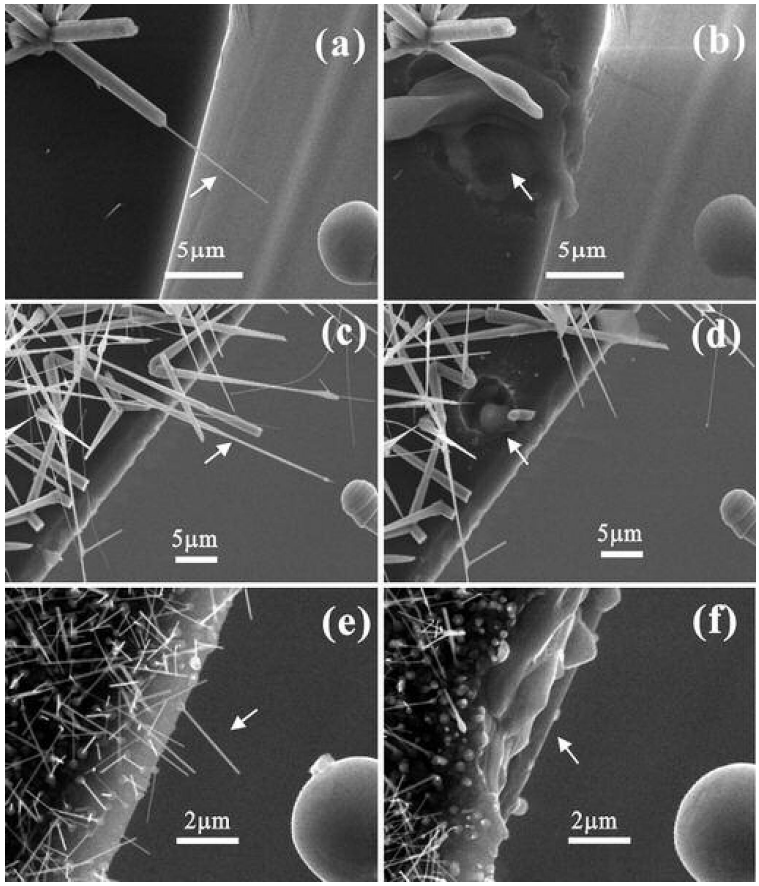

Figure 4. SEM images showing the morphology change of the high-resistance 1D ZnO nanostructures before and after the measurements: (a and b) the pencil-like; (c and d) the agave-like; (e and f) the hierarchical structures.

point (individual 1D ZnO nanostructure) configuration. The simulation is based on Poisson's equation for scalar electric potential U ($E = -\text{grad}U$, where E is the electric field intensity vector):

$$\frac{\partial}{\partial r}\left(\varepsilon_r \frac{\partial U}{\partial r}\right) + \frac{\partial}{\partial z}\left(\varepsilon_z \frac{\partial U}{\partial z}\right) = -\rho \qquad (1)$$

where ε_r and ε_z are the electrical permittivity of the ZnO along the r and z axis, respectively, and ρ is the electric charge density. In the simulations, the following parameters were used (*i.e.*, the radius of curvature of the anode probe $R = 1.5$ μm, the electrical permittivity of ZnO and Si substrate are 7.9[24] and 11.8,[24] respectively). The anode emitter separation is 2 μm. The models representing the 1D ZnO nanostructures were defined as those seen in Figure 1. The parameters are given in Table I for those of the emitters tested. Typical E_{apex} values under a bias of 100 V are also given in Table I. Clearly, the E_{apex} values are varied. Typically, the emitters with higher aspect ratio have larger E_{apex} values. From the experimental results, we plotted two curves in Figure 7b, showing how the emission current (I_E) at a same E_{apex} of 1.29×10^3 MV/m is related to the R values. Though the E_{apex} is the same, the I_E is varied greatly. Clearly, the changing behavior of I_E and R is reversed, implying that the resistance governs the emission of the 1D nanostructures.

Indeed, the resistance obtained in our measurements may be contributed to three parts, the contact junction between the Si substrate and the ZnO nanostructure (R_{Si-ZnO}), the body of the ZnO nanostructure (R_{body}), and the contact resistance between ZnO−W (R_{ZnO-W}). However, no significant R_{ZnO-W} is expected to exist in our measurements. Namely, the ZnO−W contact may well be of an ohmic type, as reported by Liu *et al.*[25] Therefore, the resistance difference may come from R_{Si-ZnO} or R_{body}. For the present study, the junction of the 1D nanostructure and Si substrate is actually a Si/a-C/ZnO sandwich joint.[17] The existence of a-C between the Si and ZnO may lower the Schottky barrier at the joint. Panels a and b of Figure 8, respectively, give the band diagrams of the Si/ZnO and Si/a-C/ZnO interfaces for illustrating the possible mechanism. Since the Si wafer we used is heavily n-doped, we treated it as a metallic substrate with a work function of 4.3 eV.[24] According to ref 22, the work function of ZnO is ~5.2 eV. In general, the Schottky barrier at the Si/ZnO (metallic−semiconductor) interface has a finite height (*i.e.*, 1.7 eV; Figure 8a). With a-C addition, which has a band gap of ~1.55 eV,[26] the electrons at the Femi level (E_F) of the metallic substrate may see a relatively low potential (0.9 eV). After injecting into the a-C film, electrons may transport and finally arrivie at the a-C/ZnO interface. At this interface, the potential barrier height may be estimated to be 0.9 eV (band gap of ZnO = 3.37 eV[27]). Under this consideration, the relative high potential barrier at the Si/ZnO interface was "disported" into two relative low barriers. The electron tunneling efficiency can be significantly enhanced. Thus, it is reasonable to propose that the resistance difference may mainly be due to the difference in R_{body}.

R_{body} is determined by both geometrical shape and resistivity. Some recent works have demonstrated that the conductance of ZnO may be dominated by the conduction of surface layer (typically 5−25 nm in thickness).[28] We, thus, assume that this effect plays a major role in the conductivity of the ZnO 1D structure. Derivations were carried out for calculating the conductivity of each type of the nanostructures based on the models schematically illustrated in Figure 1. In Figure 1a, $r-x$ coordinates were set up, where r and x represent the radius and the length of the nanostructure, respectively. Thus, we take the surface conduction shell with an inner and outer radius of $r(x)$ and $r(x) + t$, respectively. Here t is the thickness of the surface conduction layer. On the basis of this assumption and further assuming the conductivity of the nanostructure is uniform along the surface, the conductivity is given by

$$\sigma = \frac{1}{R}\int_0^l \frac{dx}{\pi[(r(x)+t)^2 - r^2(x)]} \quad (2)$$

where R is the resistance of the nanostructure, σ is the conductivity, and l is the length of the nanostructure.

For the agave-like structure (Figure 1a), the conductivity σ_a can be obtained from eq 2

$$\sigma_a = \frac{h_1}{2tR_a(r_2 - r_1)\pi}\ln\left(\frac{2r_2 - t}{2r_1 - t}\right) \quad (3)$$

where the parameters of r_1, r_2, and h_1 are corresponding to the model given in Figure 1a, R_a is the measured resistance of agave-like structure; t is the thickness of the surface conduction layer.

Similarly, for the hierarchical structure, the conductivity σ_h can be expressed as

$$\sigma = \frac{1}{R_h}\left(\frac{h_1}{t\pi(2r_1 - t)} + \frac{h_2}{t\pi(2r_2 - t)}\right) \quad (4)$$

where the parameters of h_1, h_2, r_1, and r_2 are corresponding to the model given in Figure 1b. According to Figure 1c, the pencil-like structure can be assumed to be the combination of the hierarchical structure and the agave-like structure. Thus, its surface conductivity can be expressed as

$$\sigma = \frac{1}{R_p}\left(\frac{h_1}{2t(r_2 - r_1)\pi}\ln\left(\frac{2r_2 - t}{2r_1 - t}\right) + \frac{h_2}{t\pi(2r_3 - t)}\right) \quad (5)$$

Then, we calculated the conductivity (σ) values using the resistance values and the dimensional parameters measured for each individual nanostructure by SEM (Table I). The results of the calculation are listed in Table II. They reveal that the conductivity of the nanostructure is rather different, which may be caused by the surface defect density. Generally, the ZnO surface is rich in defect, predominantly oxygen vacancy. These defects will contribute to the scattering and trapping of charge carriers and thus affect the conductivity.[28,29]

From the results presented above, it is obvious that the nanostructures with lower resistance and thus higher conductivity have better field emission performance, that is, having lower turn-on and threshold field for electron emission. This is because they have a better supply of electrons to the emitting surface. On the other hand, the nanostructure having low conductivity seems to act like an insulator, so that they may have an electrical breakdown event before stable emission current may be observed. This principle is specifically applicable to those nanostructures with very high resistance (*i.e.*, the pencil-like nanostructures, No. 5 nanostructure of the agave-like and the hierarchical structures), and no emission current was detected. The high-resistance ZnO nanostructures act as a dielectric, and

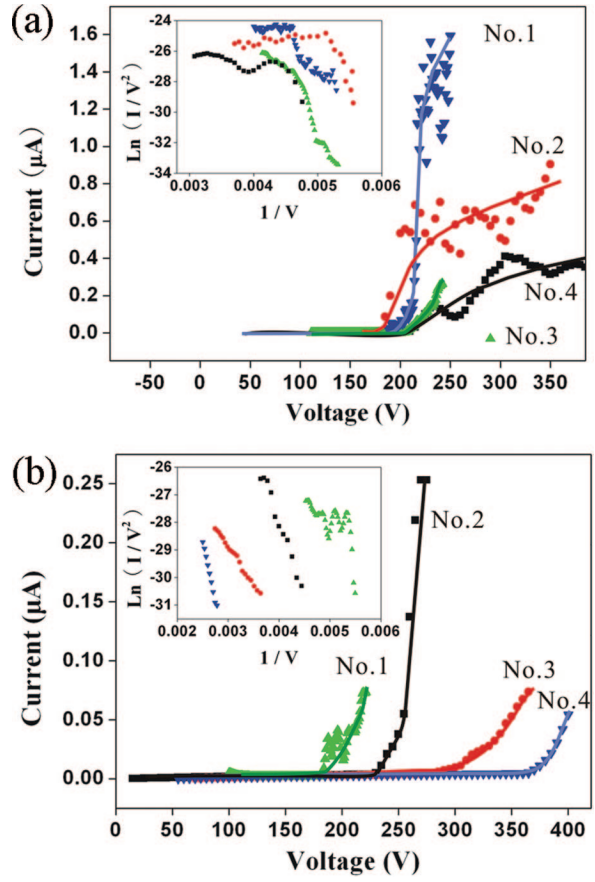

Figure 5. Typical field emission *I*–*V* curves of the agave-like (a) and the hierarchical structures (b). Insets are the corresponding F–N curves.

an electrical breakdown[30] may be induced by the high electric fields (*i.e.*, 250 MV/m applied in the measurements). Typically, the breakdown may cause an arcing, so that holes can be observed near the broken nanostructure (arrowed in the Figure 4b,d,f). The duration of the electrical breakdown is too short (~10^8 s), so that it was not detected by our test sys-

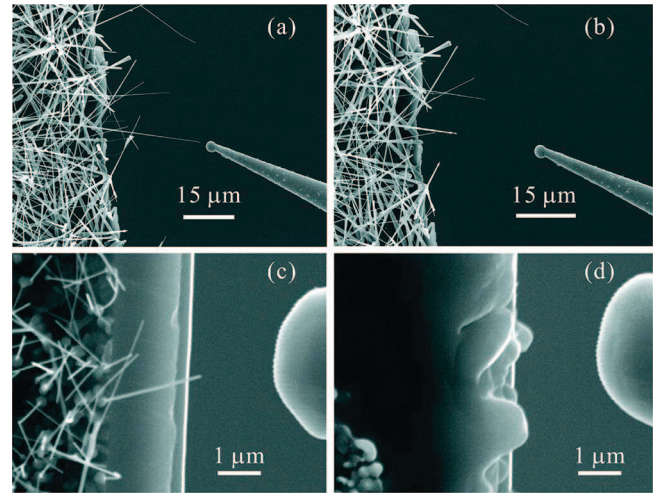

Figure 6. SEM images showing the morphology change of the 1D ZnO nanostructures before and after the maximum field emission current tests: (a and b) the agave-like; (c and d) the hierarchical structures.

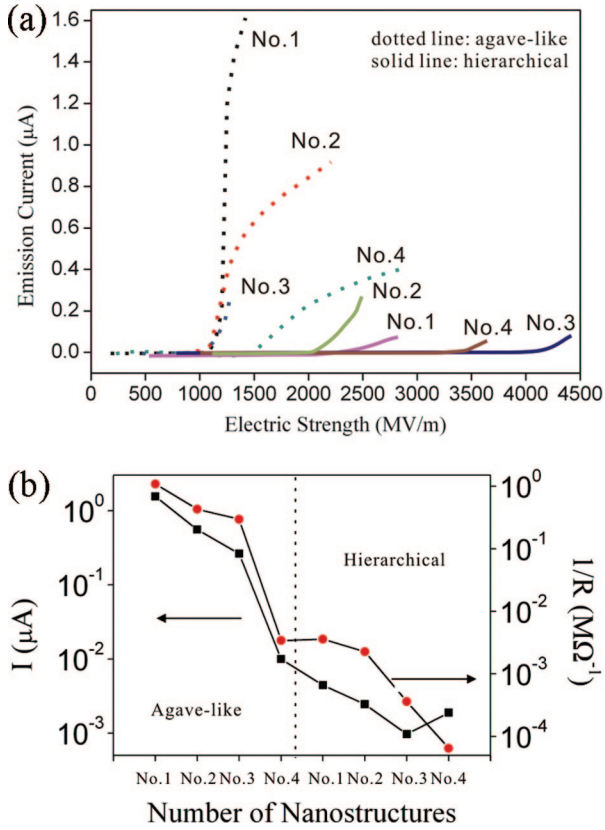

Figure 7. (a) Typical field emission *I*−*E* curves of the agave-like (dashed line) and the hierarchical structures (solid line); (b) variation of emission current (at a same E_{apex} of 1.29 × 10^3 MV/m) and *R* values for the emitters. A dashed line was used to separate the curves of the agave and the hierarchical structures.

tem. In addition, the variation of resistance in a single emitting nanostructure may lead to different initiation behavior of a vacuum breakdown event. According to Xu *et al.*,[31] the field emission induced breakdown is initiated by the creation of ionizable medium. The medium is derived from localized melting or vaporization source, here from a specific region in a single emitting nanostructure. This is because the local joule heating $Q = I^2R$ (where *I* is equal to the emission current and *R* the local resistor) plays an important role in this process. A vacuum breakdown event may be initiated by melting or vaporization at the local positions, where they

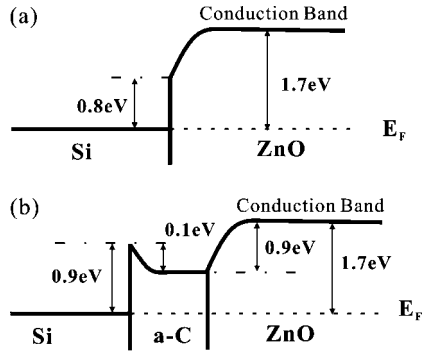

Figure 8. Band diagrams of the Si/ZnO (a) and Si/a-C/ZnO (b) interfaces.

TABLE II. Calculated Conductivity for the 1D ZnO Nanostructures

nanostructures		conductivity (Ω^{-1} m^{-1})
agave-like	No.1	3.37 × 10^3
	No.2	1.50 × 10^3
	No.3	1.74 × 10^3
	No.4	7.13
	No.5	1.66 ×10^{-2}
hierarchical	No.1	2.57
	No.2	1.86
	No.3	0.348
	No.4	8.79 ×10^{-2}
	No.5	1.75 ×10^{-3}
pencil-like	No.1	4.23
	No.2	1.44 ×10^{-2}
	No.3	6.02 ×10^{-3}
	No.4	4.42 ×10^{-4}
	No.5	5.04 ×10^{-5}

have the highest resistance. As may be seen from Figure 6b, the agave-like emitters were broken near the tip apexes because their diameter was getting smaller and thus the resistance was getting larger. Joule heating is the largest at the tip apex in this case. For the hierarchical emitters, the resistance of the junction between the trunk and top nanowire seems to be the largest in these nanostructures. The breakdown destroyed the whole emitter as well as its surroundings (Figure 6d) since the trunk is rather short (200 nm).

The findings from the present study present a new consideration that should be taken into account in a practice of device design. It is widely known that uniform emission is required for large-area device application. The uniformity on geometrical structure in an emitting array has been the main factor that one often considers. However, our present finding strongly indicates that the uniform conductivity is equally important. A workable device may not be realized, even though well-aligned arrays of nanostructure with uniform geometry are achieved.

CONCLUSIONS

In summary, electrical conduction and field emission measurements were performed on individual ZnO 1D nanostructures of three shapes. Their conductivity, field emission properties, and vacuum breakdown behaviors have been investigated. Generally, the 1D ZnO nanostructures have obvious difference in resistance and thus conductivity from type to type. In the same type of 1D ZnO nanostructure, each individual emitter may also have variation in resistance and thus conductivity, among which a small proportion of the 1D ZnO emitters in each type may have very large resistance. Emitters with lower resistance exhibited better field emission performance. The vacuum breakdown event may be initiated at the local position of a nanoemitter,

where highest resistance exists. Also, the findings have demonstrated that the conductivity is a very important factor affecting the field emission properties. The uniformity of the conductivity of the emitters in an array is as important in ensuring the uniformity of the emission as that of the geometrical factors. The findings enhance the understanding of the field emission from the 1D ZnO emitters.

TABLE III. Growth Conditions for the 1D ZnO Nanostructures

	growth conditions				
nanostructures	a-C thickness (nm)	*T* (K)	*t* (min)	pressure (Pa)	gas flow (sccm)
agave-like	150	1250	30	9.1×10^4	N_2: 300
hierarchical	50		5		Ar: 800
pencil-like	50		30		N_2: 300

METHODS

The 1D ZnO agave-like structures, pencil-like structures, and hierarchical structures were prepared by using a thermal chemical vapor deposition process. Heavily n-doped Si wafers coated with amorphous carbon (a-C) films were used as substrates. The detailed growth conditions for the 1D ZnO nanostructures are listed in Table III.

The electrical and field electron emission measurements were performed by employing a modified SEM system, which is equipped with a precisely manipulated (2 μm per step) anode probe (tungsten tip with clean surface). A picoammeter with power supply (Keithley 6487) was employed for the tests. The typical vacuum condition for the tests was $\sim 10^{-6}$ Torr. To study the electrical conduction characteristic of the 1D ZnO nanostructures, the microprobe was moved to attach their apexes. A sweep voltage of 0−1 V was applied between the Si substrate and the microprobe. Current−voltage (*I*−*V*) curves were obtained, which are used for calculation of resistances. After the electrical conduction measurements, the microprobe was moved backward for a step of ~2 μm. Then field electron emission measurements were performed.

Acknowledgment. The authors gratefully acknowledge the financial support of the project from the National Natural Science Foundation of China (Grant Nos. U0634002, 60601019, 60771055, 50725206, 60571035), Science and Technology Ministry of China (Grant Nos. 2003CB314701, 2007CB935501, 2008AA03A314), Education Ministry of China, the Science and Technology Department of Guangdong Province, the Education Department of Guangdong Province, and the Science and Technology Department of Guangzhou City. J.C.S. is also thankful for the support of the projects from the Natural Science Foundation of Guangdong Province (Grant No. 06300340) and Sun Yat-sen University. The authors also thank Mr. X.D. Shan and Dr. Z.M. Liao of Peking University for their kind assistance in TEM analysis.

REFERENCES AND NOTES

1. Lee, C. J.; Lee, T. J.; Lyu, S. C.; Zhang, Y.; Ruh, H.; Lee, H. J. Field Emission from Well-Aligned Zinc Oxide Nanowires Grown at Low Temperature. *Appl. Phys. Lett.* **2002**, *81*, 3648–3650.
2. Zhu, Y. W.; Zhang, H. Z.; Sun, X. C.; Feng, S. Q.; Xu, J.; Zhao, Q.; Xiang, B.; Wang, R. M.; Yu, D. P. Efficient Field Emission from ZnO Nanoneedle Arrays. *Appl. Phys. Lett.* **2003**, *83*, 144–146.
3. Banerjee, D.; Jo, S. H.; Ren, Z. F. Enhanced Field Emission of ZnO Nanowires. *Adv. Mater.* **2004**, *16*, 2028–2032.
4. Li, Y. B.; Bando, Y.; Golberg, D. ZnO Nanoneedles with Tip Surface Perturbations: Excellent Field Emitters. *Appl. Phys. Lett.* **2004**, *84*, 3603–3605.
5. Fang, X. S.; Bando, Y.; Gautam, U. K.; Ye, C. H.; Golberg, D. Inorganic Semiconductor Nanostructures and Their Field-Emission Application. *J. Mater. Chem.* **2008**, *18*, 509–522.
6. Wang, X. D.; Zhou, J.; Lao, C. S.; Song, J. H.; Xu, N. S.; Wang, Z. L. *In Situ* Field Emission of Density-Controlled ZnO Nanowire Arrays. *Adv. Mater.* **2007**, *19*, 1627–1631.
7. Yang, Y. H.; Wang, B.; Xu, N. S.; Yang, G. W. Field Emission of One-Dimensional Micro- and Nanostructures of Zinc Oxide. *Appl. Phys. Lett.* **2006**, *89*, 043108.
8. Zhao, Q.; Zhang, H. Z.; Zhu, Y. W.; Feng, S. Q.; Sun, X. C.; Xu, J.; Yu, D. P. Morphological Effects on the Field Emission of ZnO Nanorod Arrays. *Appl. Phys. Lett.* **2005**, *86*, 203115.
9. Wang, R. C.; Liu, C. P.; Huang, J. L.; Chen, S.-J.; Tseng, Y.-K.; Kung, S.-C. ZnO Nanopencils; Efficient Field Emitters. *Appl. Phys. Lett.* **2005**, *87*, 013110.
10. Zhao, Q.; Xu, X. Y.; Song, X. F.; Zhang, X. Z.; Yu, D. P.; Li, C. P.; Guo, L. Enhanced Field Emission from ZnO Nanorods *via* Thermal Annealing in Oxygen. *Appl. Phys. Lett.* **2006**, *88*, 033102.
11. Xu, C. X.; Sun, X. W.; Chen, B. J. P. Field Emission from Gallium-Doped Zinc Oxide Nanofiber Array. *Appl. Phys. Lett.* **2004**, *84*, 1540–1542.
12. Li, L.; Pan, S. S.; Dou, X. C.; Zhu, Y. G.; Huang, X. H.; Yang, Y. W.; Li, G. H.; Zhang, L. D. Direct Electrodeposition of ZnO Nanotube Arrays in Anodic Alumina Membranes. *J. Phys. Chem. C* **2007**, *111*, 7288–7291.
13. Eustis, S.; Meier, D. C.; Beversluis, M. R.; Nikoobakht, B. Analysis of Copper Incorporation into Zinc Oxide Nanowires. *ACS Nano* **2008**, *2*, 368–376.
14. Ramgir, N. S.; Mulla, I. S.; Vijayamohanan, K.; Late, D. J.; Bhise, A. B.; More, M. A.; Joag, D. S. Ultralow Threshold Field Emission from a Single Multipod Structure of ZnO. *Appl. Phys. Lett.* **2006**, *88*, 042107.
15. Yeong, K. S.; Maung, K. H.; Thong, J. T. L. The Effects of Gas Exposure and UV Illumination on Field Emission from Individual ZnO Nanowires. *Nanotechnology* **2007**, *18*, 185608.
16. Huang, Y. H.; Bai, X. D.; Zhang, Y.; Qi, J. J.; Gu, Y. S.; Liao, Q. L. Field-Emission Properties of Individual ZnO Nanowires Studied *In Situ* by Transmission Electron Microscopy. *J. Phys.: Condens. Matter* **2007**, *19*, 176001.
17. Yang, Y. H.; Wang, C. X.; Wang, B.; Li, Z. Y.; Chen, J.; Chen, D. H.; Xu, N. S.; Yang, G. W.; Xu, J. B. Radial ZnO Nanowire Nucleation on Amorphous Carbons. *Appl. Phys. Lett.* **2005**, *87*, 183109.
18. Yang, Y. H.; Wang, C. X.; Wang, B.; Xu, N. S.; Yang, G. W. ZnO Nanowire and Amorphous Diamond Nanocomposites and Field Emission Enhancement. *Chem. Phys. Lett.* **2005**, *403*, 248–251.
19. Yang, Y. H.; Wang, B.; Yang, G. W. Growth Mechanisms of One-Dimensional Zinc Oxide Hierarchical Structures. *Nanotechnology* **2006**, *17*, 5556–5560.
20. Zhang, Z. Y.; Jin, C. H.; Liang, X. L.; Chen, Q.; Peng, L. M. Current−Voltage Characteristics and Parameter Retrieval of Semiconducting Nanowires. *Appl. Phys. Lett.* **2006**, *88*, 073102.
21. Zhang, Z. Y.; Yao, K.; Liu, Y.; Jin, C. H.; Liang, X. L.; Chen, Q.; Peng, L. M. Quantitative Analysis of Current−Voltage Characteristics of Semiconducting Nanowires: Decoupling of Contact Effects. *Adv. Funct. Mater.* **2007**, *17*, 2478–2489.
22. Bai, X. D.; Wang, E. G.; Gao, P.; Wang, Z. L. Measuring the Work Function at a Nanobelt Tip and at a Nanoparticle Surface. *Nano Lett.* **2003**, *3*, 1147–1150.
23. She, J. C.; He, H.; Deng, S. Z.; Chen, Jun; Xu, N. S.; Huq, S. E.; Wang, L. Arrays of Vacuum Microdiodes Using Uniform Diamondlike-Carbon Tip Apexes. *Appl. Phys. Lett.* **2006**, *89*, 233518.

24. Liu, E. K.; Zhu B. S.; Luo, J. S. *Semiconductor Physics*; National Defense Industry Press: Beijing, 1994; pp 179 and 367−369.
25. Liu, Y.; Wang, S.; Zhang, Z. Y.; Peng, L. M.; Shi, L.; Li, Q. Measuring the Electrical Characteristics of Individual Junctions in the SnO_2 Capped ZnO Nanowire Arrays on Zn Substrate. *Appl. Phys. Lett.* **2008**, *92*, 033102.
26. Xu, N. S.; Chen, Jian; She, J. C.; Deng, S. Z.; Chen, J. The Intrinsic Relation between Field Electron Emission and Structure Characteristics of Amorphous Diamond Film. *J. Phys. D: Appl. Phys.* **2000**, *33*, 2568–2572.
27. Özgür, Ü.; Alivov, Y. I.; Liu, C.; Teke, A.; Reshchikov, M. A.; Doğan, S.; Avrutin, V.; Cho, S. J.; Morkoçd, H. A Comprehensive Review of ZnO Materials and Devices. *J. Appl. Phys.* **2005**, *98*, 041301.
28. Weber, D. H.; Beyer, A.; Volkel, B.; Golzhauser, A.; Schlenker, E.; Bakin, A.; Waag, A. Determination of the Specific Resistance of Individual Freestanding ZnO Nanowires with the Low Energy Electron Point Source Microscope. *Appl. Phys. Lett.* **2007**, *91*, 253126.
29. Chang, P. C.; Fan, Z. Y.; Chien, C. J.; Stichtenoth, D.; Ronning, C.; Lu, J. G. High-Performance ZnO Nanowire Field Effect Transistors. *Appl. Phys. Lett.* **2006**, *89*, 133113.
30. Whitehead, S. *Dielectric Breakdown of Solids*; Clarendon Press: Oxford, 1951.
31. Xu, N. S.; Latham, R. V. Electron Emission Based Breakdown Mechanisms In *High Voltage Vacuum Insulator: Basic Concepts and Technological Practice*; Latham, R. V., Ed.; Academic Press: London, 1995; pp 176−179.